



RESEARCH LETTER

10.1002/2014GL060519

Key Points:

- Downslope sediment transport is important for smoothing of steep bathymetry
- Excavated surfzone holes filled at rates correlated with bed shear stress
- Morphological diffusivity inferred from observations is consistent with theory

Correspondence to:

M. Moulton,
mmoulton@whoi.edu

Citation:

Moulton, M., S. Elgar, and B. Raubenheimer (2014), A surfzone morphological diffusivity estimated from the evolution of excavated holes, *Geophys. Res. Lett.*, *41*, doi:10.1002/2014GL060519.

Received 29 MAY 2014

Accepted 12 JUN 2014

Accepted article online 18 JUN 2014

A surfzone morphological diffusivity estimated from the evolution of excavated holes

Melissa Moulton¹, Steve Elgar¹, and Britt Raubenheimer¹

¹Department of Applied Ocean Physics and Engineering, Woods Hole Oceanographic Institution, Woods Hole, Massachusetts, USA

Abstract Downslope gravity-driven sediment transport smooths steep nearshore bathymetric features, such as channels, bars, troughs, cusps, mounds, pits, scarps, and bedforms. Downslope transport appears approximately as a diffusive term in the sediment continuity equation predicting changes in bed level, with a morphological diffusivity controlling the rate of seafloor smoothing. Despite the importance of surfzone sediment transport and morphological evolution, the size of the downslope transport term in nearshore models varies widely, and theories have not been tested with field measurements. Here observations of the infill of large excavated holes in an energetic inner surf zone provide the first opportunity to infer the morphological diffusivity in the field. The estimated diffusion coefficient is consistent with a theoretical bedload morphological diffusivity that scales with the three-halves power of the representative bed shear stress.

1. Introduction

The coupling of surfzone waves, currents, and bathymetry leads to complex patterns of sediment transport and morphological evolution. Nearshore sediment transport results in beach erosion and accretion [Aubrey, 1979], the migration of sandbars [Thornton *et al.*, 1996; Gallagher *et al.*, 1998; Plant *et al.*, 1999; Ruessink *et al.*, 2000; Hoefel and Elgar, 2003; Henderson *et al.*, 2004], and the evolution of rip current channels [Falqués *et al.*, 2000; van Enckevort and Ruessink, 2003; MacMahan *et al.*, 2008; Garnier *et al.*, 2013], and provides a mechanism for the movement of pollution and biota between land and the inner shelf [Jumars and Nowell, 1984; Feng *et al.*, 2013]. Sediment transport parameterizations and quantitative transport estimates vary considerably (see Amoudry and Souza [2011] for a review), but most theories and numerical models include a component of sediment transport in the direction of the instantaneous near-bed velocity (in response to fluid drag) and a downslope component (in response to gravity). Downslope transport appears (to first order) as a diffusive term in the sediment continuity equation used to predict temporal changes in the bed elevation [Trowbridge and Young, 1989; Kovacs and Parker, 1994; Caballeria *et al.*, 2002] and acts to smooth the surfzone seafloor. The “morphological diffusivity,” related to the size of the downslope transport, is important to the evolution of steep nearshore features, including sandbars, cusps, troughs, channels, mounds, pits, scarps, and bedforms [Douglass, 1995; van de Kreeke *et al.*, 2002; Garnier *et al.*, 2006], and is a mechanism by which equilibrium beach states are reached [Bailard, 1981; Dean, 1991; Calvete *et al.*, 2005; Garnier *et al.*, 2008].

Despite the tremendous importance of surfzone sediment transport and shoreline morphological evolution, numerical models have limited skill simulating observations, and the impact of bed slope on sediment transport in the field has not been tested [Garnier *et al.*, 2008]. There are few field observations of the evolution of steep surfzone bathymetric features, partially because it is difficult to make accurate measurements of sediment transport and bed evolution for steep morphologies that change rapidly under energetic conditions. Here, the surfzone seafloor is perturbed artificially to allow investigation of the morphological evolution of steep bathymetric features. Large holes (initially about 10 m wide and 2 m deep) were excavated in the inner surf zone of an ocean beach (Figure 1), and waves, currents, and the evolving bathymetry were measured. The holes evolve predominantly by downslope sediment transport that can be modeled as a diffusive process, and thus the perturbations provide an opportunity to estimate the morphological diffusivity that best explains the observed seafloor evolution. The morphological diffusivity estimated from the evolution of the holes is consistent with a bedload transport theory for which the diffusivity is proportional to the three-halves power of the bed shear stress.



Figure 1. Backhoe excavating a hole in the inner surf zone near Duck, NC, at low tide.

2. Field Observations

Four large holes were excavated (Figure 1) in the inner surf zone. The mean water depth surrounding the holes was 1.5 m, and the tidal range was approximately 1 m. The initial (ranging from several hours to several days after excavation) bathymetry of each hole was surveyed with a surfboard-mounted GPS-sonar system and a diver-carried GPS-pole system, yielding a set of bed-level observations for each hole (Figure 2, squares). The holes were approximately Gaussian (Figure 2, Gaussian fit to survey shown with contours in Figure 2a and curves in Figures 2b and 2c) and initially were between 1.9 and 2.7 m deep relative to an ambient bed elevation

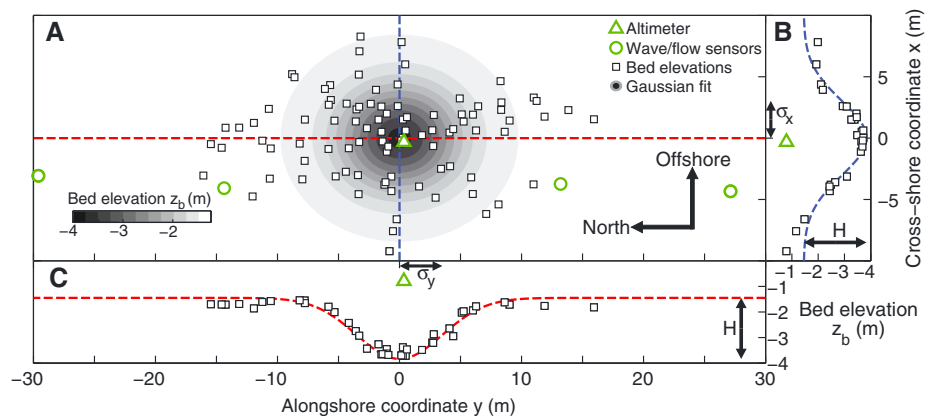


Figure 2. (a) Plan view of altimeter location (green triangle near the center), wave and velocity sensor locations (circles), bed elevation survey locations (squares), and Gaussian fit to surveyed bed elevations (grey-scale contours every 0.25 m) for one of the excavated holes as a function of cross shore (x) and alongshore (y) coordinates. The hole center is located at $x = 0$ (red dashed curve) and $y = 0$ (blue dashed curve). (b) Bed elevation z_b versus x for surveyed bed elevations near $y = 0$ (squares, plotted for $|y| < 2$ m) and for the Gaussian fit at $y = 0$ (dashed blue curve). (c) Bed elevation z_b versus y for surveyed bed elevations near $x = 0$ (squares, plotted for $|x| < 2$ m) and for the Gaussian fit at $x = 0$ (dashed red curve). The depth of the hole relative to ambient bed elevation ($H = 2.4 \pm 0.2$ m) and the cross shore and alongshore standard deviations ($\sigma_x = 3.0 \pm 0.3$ m and $\sigma_y = 3.5 \pm 0.4$ m) from the Gaussian fit (95% confidence intervals on the fit parameters are reported) are shown with arrows.

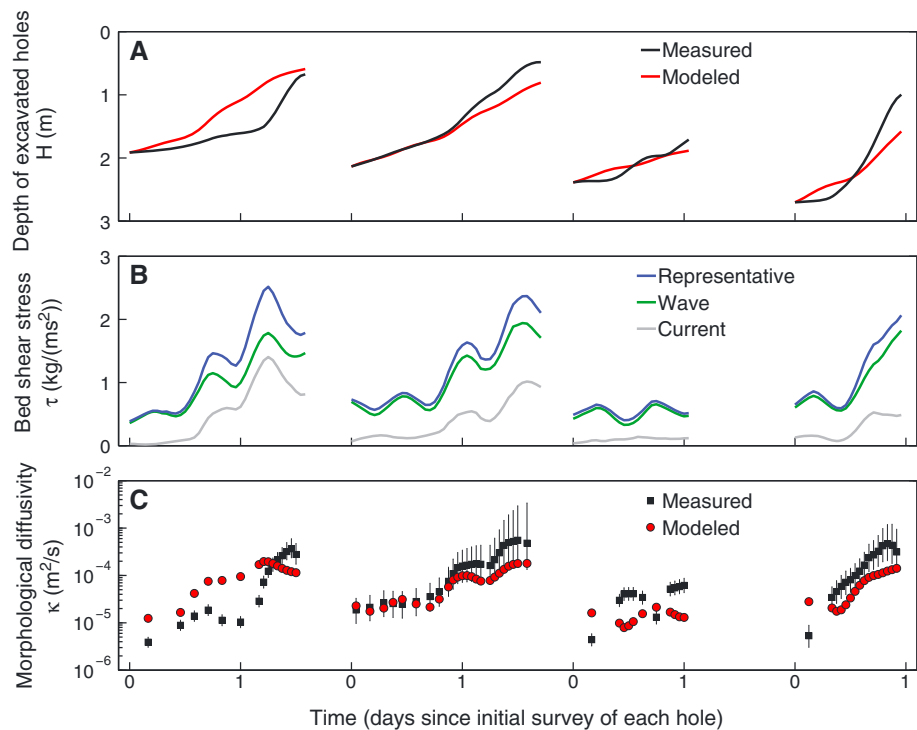


Figure 3. (a) Depth of excavated holes (m), (b) bed shear stress ($\text{kg}/(\text{ms}^2)$), and (c) morphological diffusivity (m^2/s) versus time (days since initial survey of each hole). The measured depth of the excavated holes (black curves in Figure 3a) was used with Gaussian fits to initial surveys (Figure 2) to infer a morphological diffusivity (black squares in Figure 3c; error bars are 95% confidence intervals based on initial survey fits) each time the hole filled by a measurable amount (0.05 m, one-half the profiler bin size). A bedload morphological diffusivity theory (6) with $A = 12$ [Soulsby and Damgaard, 2005] was used with the representative shear stress estimate (blue curves in Figure 3b, derived from the wave- (green curves) and current- (grey curves) associated stresses) to model the time evolution of the morphological diffusivity (red circles in Figure 3c) for the same time windows as for the data. The modeled coefficient was used to predict the hole depth evolution (red curves in Figure 3a, model initial condition is the Gaussian fit to each initial survey).

(Figure 3a, initial values of black curves), with widths (defined as 4 times the standard deviation of the Gaussian shape from a fit to an elliptical Gaussian) between 14 and 17 m in the alongshore (Figure 2c) and between 9 and 14 m in the cross shore (Figure 2b). The root-mean-square (RMS) differences between the observed elevations and the Gaussian fits for the four holes (in the order shown in Figure 3) are 0.28 m, 0.17 m, 0.25 m (the survey shown in Figure 2), and 0.17 m, approximately the same size as the expected RMS measurement error (0.20 m) for the watercraft and diver survey methods [Moulton *et al.*, 2014]. Shortly after each excavation, an altimeter was deployed above (near the ambient bed elevation) the center of the hole (triangle in Figure 2). The altimeters sampled continuously (2 MHz acoustic profilers, 1 min average samples, 10 cm vertical bins), and backscatter amplitudes (not shown) were used to make hourly estimates of the seafloor elevation. A 7 h running mean was applied to the hourly seafloor elevation estimates to remove migrating bedforms (e.g., megaripples) from the signal. Waves and currents used to estimate bottom stress were measured with 4 to 6 acoustic Doppler velocimeter and pressure gage pairs (sampled at 2 Hz) deployed 10 to 30 m apart near each hole (e.g., circles in Figure 2a) with transducers approximately 0.7 m above the bed. Significant wave heights (defined as 4 times the sea surface elevation standard deviation) near the holes ranged from 0.2 to 1.2 m, and mean current speeds ranged from 0.1 to 1.2 m/s. The median grain diameter (d_{50}) near the holes was 0.3 mm.

3. Theoretical Morphological Diffusivity

Sediment in the surf zone is transported as bed load (in which grains roll, slide, or saltate near the bed) and suspended load (in which grains move in the water column). Based on the ratio of the turbulent vertical velocity fluctuations to the sediment fall velocity [Gonzalez-Rodriguez and Madsen, 2011], sediment transport

was dominated by bed load for the field conditions considered here. The volumetric bedload transport \mathbf{Q} can be determined from an along-bed force balance on a sediment grain in the presence of waves, currents, and a sloping bed [Bagnold, 1966; Bailard, 1981; Trowbridge and Young, 1989; Fredsøe and Deigaard, 1992; Nielsen, 1992; Kovacs and Parker, 1994; Soulsby, 1997; Soulsby and Damgaard, 2005; Amoudry and Souza, 2011] and can be expressed as the sum of a component of transport in the instantaneous flow direction (owing to fluid drag on a flat bed, referred to as “flat-bed transport” \mathbf{Q}_0) and a component downslope (owing to the presence of a sloping bed, referred to as “downslope transport” \mathbf{Q}_s).

Most bedload formulations relate the transport to a power of the bed shear stress [Amoudry and Souza, 2011]. Thus, a bedload transport relationship [Meyer-Peter and Müller, 1948; Soulsby and Damgaard, 2005] modified for the presence of a sloping bed [Bagnold, 1966; Bailard, 1981; Kovacs and Parker, 1994] is given by

$$\mathbf{Q} = \mathbf{Q}_0 + \mathbf{Q}_s = \frac{A}{\rho^{3/2}(s-1)g} \tau^{1/2} (\tau - \tau_{cr}) \left[\frac{\boldsymbol{\tau}}{\tau} - \frac{\nabla z_b}{\tan \phi} \right] \quad (1)$$

where $\rho = 1025 \text{ kg/m}^3$ is the density of seawater, $s = 2.57$ is the ratio of the density of sediment (quartz) to the density of seawater, g is the gravitational constant, A is a dimensionless coefficient [Soulsby and Damgaard, 2005], τ is the magnitude of the bed shear stress, $\tau_{cr} \approx 0.17 \text{ kg/(ms}^2)$ [Shields, 1936] is a critical shear stress for initiation of motion ($\mathbf{Q} = 0$ for $\tau \leq \tau_{cr}$), ∇z_b is the gradient of the bed level, and $\phi = 32^\circ$ is the angle of repose. The unit vector $\left[\frac{\boldsymbol{\tau}}{\tau} \right]$ is oriented in the instantaneous flow direction, and the vector $\left[-\frac{\nabla z_b}{\tan \phi} \right]$ is directed downslope. The form of (1) relies on the assumption that the bed slope is much smaller than the angle of repose ($\left| \frac{\nabla z_b}{\tan \phi} \right| \ll 1$), which is only weakly satisfied for some of the steepest slopes of the excavated holes ($0.05 < \left| \frac{\nabla z_b}{\tan \phi} \right| < 0.50$). However, (1) is used widely and is expected to describe the first-order effects of the downslope transport. In addition, the critical shear stress is expected to vary with the bed slope, and the downslope transport may depend on the angle between the bed gradient and the flow direction [Kovacs and Parker, 1994]. These higher-order effects are neglected here.

Usually, nearshore morphology changes on time scales of storms or seasons, much longer than the period of surface gravity waves (about 10 s). Thus, often sediment transport and bed-level predictions are integrated over wave cycles, and approximations for the wave-averaged transport are used to avoid computationally expensive numerical integrations [Soulsby and Damgaard, 2005]. The total near-bed shear stress vector is approximately the sum of the shear stress from the mean current in the presence of waves $\boldsymbol{\tau}_m$ and the time-dependent shear stress vector $\boldsymbol{\tau}_w$ associated with a representative wave [Grant and Madsen, 1986; Madsen, 1994]. For (oscillatory) flat-bed transport owing to nearly sinusoidal waves perpendicular to a mean flow, the wave-averaged transport is in the direction of the mean current and goes as $\tau_w^{1/2} \tau_m$ [Soulsby and Damgaard, 2005], where τ_m is the magnitude of the mean shear stress vector and τ_w is the amplitude of the oscillating wave shear stress vector. In contrast, the downslope transport is unidirectional (downslope), and thus, the transport does not average to zero for sinusoidal waves, and the net transport is better parameterized using a representative wave current bed shear stress magnitude, $\tau_r = \max(|\boldsymbol{\tau}_m + \boldsymbol{\tau}_w|)$. Therefore, for the field conditions presented here, the wave-averaged flat-bed transport and downslope transport are expressed approximately as (numerical experiments show that errors are small)

$$\langle \mathbf{Q}_0 \rangle \approx \frac{A}{\rho^{3/2}(s-1)g} \tau_w^{1/2} \tau_m \left[\frac{\boldsymbol{\tau}_m}{\tau_m} \right] \quad (2)$$

$$\langle \mathbf{Q}_s \rangle \approx \frac{A}{\rho^{3/2}(s-1)g} \tau_r^{1/2} (\tau_r - \tau_{cr}) \left[-\frac{\nabla z_b}{\tan \phi} \right] \quad (3)$$

where $\langle \cdot \rangle$ indicates an average over a wave cycle, $\frac{1}{2\pi} \int_0^{2\pi} \cdot d(\omega t)$ and $\left[\frac{\boldsymbol{\tau}_m}{\tau_m} \right]$ is a unit vector oriented in the mean flow direction. The expression (2) [Soulsby and Damgaard, 2005] requires that $\tau_w \gg \tau_m$ and $\tau \gg \tau_{cr}$, consistent with the average field conditions considered here. For these field conditions, (3) may be simplified further by noting that $\tau_r^{1/2} (\tau_r - \tau_{cr}) \approx \tau_w^{3/2}$, but the form above shows better agreement with a wider range of field conditions.

Mass conservation equates temporal changes in bed elevation (erosion or accretion) with spatial gradients (divergences or convergences) of horizontal sediment transport

$$\frac{\partial z_b}{\partial t} + \frac{1}{(1-n)} \nabla \cdot \langle \mathbf{Q} \rangle = 0 \quad (4)$$

where z_b is the elevation of the bed and $n=0.3$ is the sediment porosity. Substituting (1) into (4) and applying the approximation in (3) yields

$$\frac{\partial z_b}{\partial t} = -\frac{1}{(1-n)} \nabla \cdot \langle \mathbf{Q}_0 \rangle + \nabla \cdot (\kappa \nabla z_b) \quad (5)$$

$$\kappa = \frac{1}{(1-n)} \frac{A}{\rho^{3/2}(s-1)g} \frac{1}{\tan \phi} \tau_r^{1/2} (\tau_r - \tau_{cr}) \quad (6)$$

The downslope transport (3) results in a diffusive term in the mass conservation equation ((4) and (5)), and the coefficient κ (6) is referred to as the morphological diffusivity. The morphological diffusivity may vary temporally as the representative shear stress changes in response to changing incident wave conditions (e.g., passage of storms) and water depths (e.g., tidal fluctuations) and spatially as the stress changes in response to bathymetrically induced circulation patterns (e.g., divergence of a mean flow over a channel). Both terms in (5) may be important for the evolution of nearshore bathymetric features. For example, the offshore migration of sandbars during storms primarily is the result of offshore flowing currents that are maximum near the crest of the bar (leading to divergences in \mathbf{Q}_0) [Thornton *et al.*, 1996; Gallagher *et al.*, 1998], but the downslope transport \mathbf{Q}_S may be an important control on the bar height and slope, which impact the bar migration speed [Trowbridge and Young, 1989].

4. Methods

4.1. Inferring a Morphological Diffusivity From Evolving Bathymetry

The evolution of the excavated holes is expected to be dominated by the diffusive term (related to the downslope transport \mathbf{Q}_S) for several reasons. Although the instantaneous downslope transport \mathbf{Q}_S is (according to (1)) smaller than the instantaneous flat-bed transport \mathbf{Q}_0 , the wave-averaged downslope transport may be larger than the wave-averaged flat-bed transport. In particular, the wave-averaged flat-bed transport (2) is small for sinusoidal oscillatory waves and small mean flows ($\tau_m < \tau_w$, Figure 3b). Although wave orbital velocities in the surf zone are skewed and asymmetric, for the conditions here they do not transport significant amounts of sediment over the relatively short periods during which the holes filled. Conservation of sediment (5) predicts that flat-bed transport owing to a diverging mean flow would lead to migration of the holes in the mean flow direction [van de Kreeke *et al.*, 2002]. However, the holes were not observed to migrate, implying bed evolution owing to diverging mean flows was small. The holes had steeply sloping sides, while the bed slope was small outside of the holes and at the hole centers, leading to large spatial gradients in the downslope flux. The downslope transport (3) scales with the combined wave and current shear stress magnitude τ_r , which (by definition) is larger than either τ_w or τ_m (Figure 3b). Thus, it is expected that the downslope term dominates the hole evolution (the second term on the right-hand side of (5) usually is larger than the first term), and the bathymetric change in time is approximated by

$$\frac{\partial z_b}{\partial t} \approx \nabla \cdot (\kappa \nabla z_b) \quad (7)$$

This balance and the measured bathymetric evolution can be used to find the diffusivity that best explains the evolution of the seafloor, similar to inverting tracer dispersion to infer hydrodynamic diffusivities [Ledwell *et al.*, 1998; Clark *et al.*, 2010].

For an approximately Gaussian bathymetry (Figure 2) evolving according to (7), the bathymetry remains a Gaussian at all times, and the morphological diffusivity can be expressed as an analytical function of the hole depth and width. An elliptical Gaussian hole has the form

$$z_b(x, y, t) = -H(t) \exp \left[-\left(\frac{x^2}{2\sigma_x^2(t)} + \frac{y^2}{2\sigma_y^2(t)} \right) \right] + z_{amb} \quad (8)$$

where $H(t)$ is the maximum hole depth, z_{amb} is the ambient bed elevation, and $\sigma_x(t)$ and $\sigma_y(t)$ are the standard deviations of the Gaussian shape in the cross shore (x) and alongshore (y), respectively. If the hole evolves diffusively (7), the depth and standard deviations at two times t_1 and t_2 are related by

$$H(t_2) = H(t_1) \left[\left(1 + \frac{2\kappa\Delta t}{\sigma_x^2(t_1)} \right)^{-1/2} \left(1 + \frac{2\kappa\Delta t}{\sigma_y^2(t_1)} \right)^{-1/2} \right] \quad (9a)$$

$$\sigma_x(t_2) = \sigma_x(t_1) \left(1 + \frac{2\kappa\Delta t}{\sigma_x^2(t_1)} \right)^{1/2} \quad (9b)$$

$$\sigma_y(t_2) = \sigma_y(t_1) \left(1 + \frac{2\kappa\Delta t}{\sigma_y^2(t_1)} \right)^{1/2} \quad (9c)$$

where $\Delta t = t_2 - t_1$. If the morphological diffusivity κ varies between times t_1 and t_2 (e.g., owing to changing incident wave conditions) and over the spatial domain (e.g., owing to flows diverging over the hole), the value of κ in (9a, 9b, 9c) may be approximated using the average value in space and time. Numerical experiments verify that this approximation leads to small errors in κ that are negligible relative to other sources of observational uncertainty.

For each hole, the depth at the center $H(t)$ (Figure 3a) is known at all times from the altimeter at the hole center (triangle in Figure 2), and the standard deviations at an initial time (arrows in Figure 2) are estimated by fitting (8) to the initial survey (black squares in Figure 2). Thus, the diffusivity can be inferred by solving (9a) for κ between times t_1 and t_2 when the depth changed by 0.05 m (half of the altimeter bin size, approximately the smallest measurable depth change). The standard deviations (8) were updated from the initial value using (9b) and (9c). The estimates of morphological diffusivity (black squares in Figure 3c) are similar if a different fraction or multiple of the bin size is used, or if a uniform time step is chosen. The error bars on these observationally inferred diffusivity estimates (Figure 3c) are the range of κ given the 95% confidence intervals on the hole depth and standard deviations. The confidence intervals on the initial conditions are based on the confidence intervals for a nonlinear regression fit of an elliptical Gaussian to the initial survey of each hole. The confidence intervals on the hole depths are based on the uncertainty associated with the depth relative to the ambient bed elevation (from the initial fit to (8), e.g., see Figure 2). The confidence interval on the initial standard deviations is found from the Gaussian fit (Figure 2), and the confidence intervals at subsequent time steps are found by updating the standard deviations (using (9b) and (9c)) with the range of inferred κ from the previous time step.

4.2. Bed Shear Stress Estimates

Observations from the four to six sensors nearest the cross-shore position of the hole centers (circles in Figure 2a) were used to estimate hourly wave, current, and representative (magnitude of the vector sum of the wave- and current-associated terms) near-bed shear stresses in the holes (Figure 3b) with a spectral wave current bottom boundary layer approach [Grant and Madsen, 1986; Madsen, 1994]. The RMS representative near-bed wave orbital (from hourly wave spectra, for frequencies < 0.25 Hz) and hourly mean velocities were used in the estimates. The shear stresses from the individual sensors were averaged, and a 7 h running mean was applied to the estimates. The roughness height $k_n = 11d_{50}$ is an average mobile-bed roughness based on best fits to observations from a previous field study at this site [Hsu et al., 2006]. This roughness value is expected to be appropriate for the environment of the excavated holes, although inner-surfzone roughness values for typical grain sizes ($0.2 < d_{50} < 0.5$ mm) range from $k_n = d_{50}$ to $k_n = 35d_{50}$, and sometimes vary with the shear velocity [Ribberink, 1998; Dohmen-Janssen et al., 2001; Nielsen, 2006; Hsu and Raubenheimer, 2006; Gonzalez-Rodriguez and Madsen, 2011]. Variation of the choice of roughness within this wide range leads to changes in the estimate of the shear stresses by up to an order of magnitude and is a major source of uncertainty in this analysis.

The near-bed shear stresses are expected to vary substantially from the shallow sides to the deep center of the hole, as wave near-bed velocities may decrease over the deeper part of the hole, leading to smaller wave shear stresses. In addition, mean currents may slow as they flow over the deeper water in the holes, also leading to smaller stresses. Separation effects also may be important, but are not considered here. To account for the deeper water in the holes, the average shear stresses in the hole (Figure 3b) were

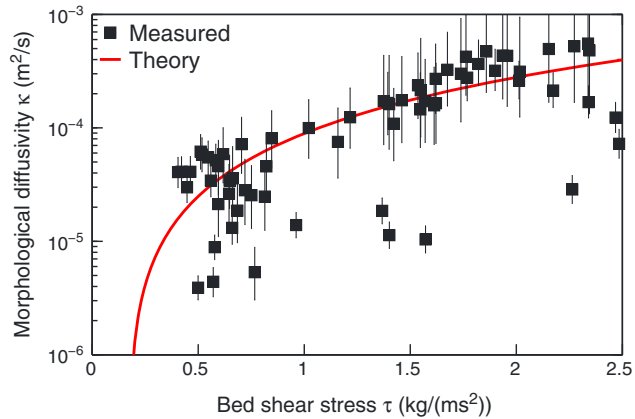


Figure 4. Morphological diffusivity (m^2/s) versus representative shear stress ($\text{kg}/(\text{ms}^2)$) for measurements (black squares; error bars are 95% confidence intervals, also see Figure 3c) and for a fit of the observed values to a bedload transport theory ((6), with a best fit $A = 24$, giving $r = 0.73$) (red curve).

approximated by multiplying the representative shear stresses estimated at the sensors on the shallow sides of the holes by the ratio of the water depth on the shallow side to the water depth at one half of the maximum hole depth (ratios ranged from 0.5 to 0.9) raised to the three-halves power. Results for the representative shear stress in the holes are similar to those using approaches that treat wave near-bed velocity evolution (wave stress reduced by the ratio of water depths to the three-halves power, green curves in Figure 3b) and flow divergence (mean stress reduced by the ratio of the water depths squared, grey curves in Figure 3b) separately.

5. Results and Discussion

The average representative shear stress estimates (blue curves in Figure 3b) were used in (6) with $A = 12$ [Soulsby and Damgaard, 2005] to model theoretical bedload morphological diffusivities (red circles in Figure 3c) for the same time windows used for the observationally inferred diffusivities (black squares in Figure 3c). The modeled morphological diffusivity is correlated with the morphological diffusivity inferred from data (compare red circles with black squares in Figure 3c). In addition, the time series of modeled diffusivities were used to predict the evolution (beginning with the initial Gaussian fit) of the depth of the holes (red curves in Figure 3a). The modeled diffusivity skillfully predicts the observed change in the seafloor elevation in the center of the holes as they fill (compare red with black curves in Figure 3a). Both observed and modeled diffusion coefficients are of order 10^{-5} to 10^{-3} m^2/s (Figure 3c), implying diffusive evolution time scales of hours to weeks for features with length scales of order 10 m. The holes filled most rapidly (and the measured and modeled diffusivities were largest) when shear stresses were larger. For example (see Figure 3), Hurricane Danielle passed offshore beginning near day 1 of the first hole, a Nor'easter produced large offshore waves near day 0.5–1.5 of the second hole, and Hurricane Igor passed offshore beginning near day 0.5 for the fourth hole. The observationally inferred diffusivities (black squares in Figures 3c and 4) are consistent with bedload transport theory (6) in which the diffusivity is proportional to the three-halves power of the shear stress (red curve in Figure 4). The representative shear stress (x axis in Figure 4) was averaged over the same time windows as the observed diffusivities, and the data were fit to the theoretical relationship (6) (red curve in Figure 4), where A is the fit parameter, yielding $A = 24$ (correlation $r = 0.73$).

While the observations are consistent with the bedload transport theory, there is some disagreement between the measured and modeled diffusivities and between the coefficient A fit to the observations ($A = 24$) and used in theory (e.g., $A = 12$, derived in Soulsby and Damgaard [2005]; see Amoudry and Souza [2011] for a review). The correlations for fits of the observed diffusivities to the theoretical relationship (6) are similar for a wide range of roughness heights (used to estimate the shear stress), while the coefficient A varies substantially. For $k_n = d_{50}$, $r = 0.70$ and $A = 65$. For $k_n = 11d_{50}$, $r = 0.73$ and $A = 24$. For $k_n = 35d_{50}$, $r = 0.74$ and $A = 14$. The diffusivity in (6) varies approximately as $\kappa \propto \tau_r^{3/2}$ (the correlation does not change significantly when τ_{cr} is set to 0, but τ_{cr} is retained in (6) for better agreement with diffusivities observed at low shear stresses). However, the

diffusivity may vary with a different power of the shear stress, e.g., at high shear stresses when suspended load may be significant and a higher-power dependence is expected [Baillard, 1981], or for other theoretical relationships that predict a lower shear stress dependence [Chen *et al.*, 2010]. For the diffusivities inferred here, the correlation for the relationship $\kappa \propto \tau_r^B$ is maximum near $B = 3/2$ ($r = 0.73$) and decreases to approximately 80% of the maximum at $B = 1/2$ ($r = 0.57$) and $B = 3$ ($r = 0.59$), suggesting that the observations are consistent with (6) and that more of the variance is explained by $B = 3/2$ than by lower or higher powers. In addition, there are errors in the modeled morphological diffusivity associated with the choice of a constant roughness height (variations in the roughness height with changes in the shear stress were not considered), with the shear stress variation with depth across the hole and with neglected possible separation effects. The inferred morphological diffusivity also has errors associated with the bathymetric sampling, deviations from the Gaussian approximation, and changes in the ambient bed elevation (accretion or erosion of the surrounding seafloor).

In some instances, particularly when the mean shear stress is large and spatially variable or if wave orbital velocities are highly asymmetrical, the divergence of the flat-bed transport may become important. For example, trenches have been observed to migrate owing to diverging tidal currents [van de Kreeke *et al.*, 2002], sandbars migrate offshore during storms owing to diverging “undertow” currents [Thornton *et al.*, 1996; Gallagher *et al.*, 1998], and the onshore migration of sandbars between storms may be driven by asymmetrical wave orbital velocities [Elgar *et al.*, 2001; Hoefel and Elgar, 2003]. Here, however, migration of the holes (which could lead to an overestimate of the diffusivity if the center (deepest part) of the hole moved away from the altimeter) was not observed by divers or in surveys. Unlike larger-scale features (e.g., 50 m wide, 100 m long rip channels) that may migrate or change shape owing to feedback between spatially varying waves, currents, and bathymetry, the 10 m diameter holes did not appear to impact the surrounding circulation in a way that led to large-scale morphological change. Instead, the results here suggest that for these steep, relatively small-scale features, downslope sediment transport is the dominant process in the hole evolution.

Despite uncertainty in the bed level and shear stress observations, the morphological diffusivity inferred from the excavated holes is consistent with a bedload transport theory in which the diffusivity scales with the bed shear stress to the three-halves power. The observations of infilling excavated holes provide the first opportunity to infer a morphological diffusivity in the surf zone and suggest that for bathymetric features with large and changing slopes, downslope gravity-driven bedload sediment transport is important to morphological evolution.

Acknowledgments

Data are available via e-mail to the corresponding author.

We thank the PVLAB field team and the staff of the U.S. Army Corps of Engineers Field Research Facility, Duck, NC, for excellent field support, and in particular Brian Scarborough for excavating ordinance-laden sediments in the surf without getting the backhoe too wet and without blowing up anything (or anyone). Funding was provided by the Assistant Secretary of Defense for Research and Engineering, a National Defense Science and Engineering Graduate Fellowship, a National Science Foundation Graduate Research Fellowship, and the Office of Naval Research. The authors thank two anonymous reviewers for their helpful comments in improving this paper.

The Editor thanks two anonymous reviewers for their assistance in evaluating this paper.

References

- Amoudry, L. O., and A. J. Souza (2011), Deterministic coastal morphological and sediment transport modeling: A review and discussion, *Rev. Geophys.*, *49*, RG2002, doi:10.1029/2010RG000341.
- Aubrey, D. G. (1979), Seasonal patterns of onshore/offshore sediment movement, *J. Geophys. Res.*, *84*(C10), 6347–6354, doi:10.1029/JC084iC10p06347.
- Bagnold, R. A. (1966), An approach to the sediment transport problem from general physics, *U.S. Geol. Surv. Prof. Paper*, *422*, 231–291.
- Bailard, J. A. (1981), An energetics total load sediment transport model for a plane sloping beach, *J. Geophys. Res.*, *86*, 10,938–10,954, doi:10.1029/JC086iC11p10938.
- Caballera, M., G. Coco, A. Falqués, and D. Huntley (2002), Self-organization mechanisms for the formation of nearshore crescentic and transverse sand bars, *J. Fluid Mech.*, *465*, 379–410, doi:10.1017/S002211200200112X.
- Calvete, D., N. Dodd, A. Falqués, and S. van Leeuwen (2005), Morphological development of rip channel systems: Normal and near-normal wave incidence, *J. Geophys. Res.*, *110*, C10006, doi:10.1029/2004JC002803.
- Chen, X., J. Ma, and S. Dey (2010), Sediment transport on arbitrary slopes: Simplified model, *J. Hydraul. Eng.*, *136*(5), 311–317, doi:10.1061/(ASCE)HY.1943-7900.0000175.
- Clark, D. B., F. Feddersen, and R. T. Guza (2010), Cross-shore surfzone tracer dispersion in an alongshore current, *J. Geophys. Res.*, *115*, C10035, doi:10.1029/2009JC005683.
- Dean, R. (1991), Equilibrium beach profiles: Characteristics and applications, *J. Coastal Res.*, *7*, 53–84.
- Dohmen-Janssen, C., W. Hassan, and J. Ribberink (2001), Mobile-bed effects in oscillatory sheet flow, *J. Geophys. Res.*, *106*(C11), 27,103–27,115, doi:10.1029/2000JC000513.
- Douglass, S. L. (1995), Estimating landward migration of nearshore constructed sand mounds, *J. Waterway, Port, Coastal, Ocean Eng.*, *121*, 247–250.
- Elgar, S., E. L. Gallagher, and R. T. Guza (2001), Nearshore sandbar migration, *J. Geophys. Res.*, *106*(C6), 11,623–11,627, doi:10.1029/2000JC000389.
- Falqués, A., G. Coco, and D. A. Huntley (2000), A mechanism for the generation of wave-driven rhythmic patterns in the surf zone, *J. Geophys. Res.*, *105*(C10), 24,071–24,088, doi:10.1029/2000JC900100.
- Feng, Z., A. Reniers, B. K. Haus, and H. M. Solo-Gabriele (2013), Modeling sediment-related enterococci loading, transport, and inactivation at an embayed nonpoint source beach, *Water Resour. Res.*, *49*(2), 693–712, doi:10.1029/2012WR012432.
- Fredsoe, J., and R. Deigaard (1992), *Mechanics of Coastal Sediment Transport*, Adv. Ser. on Ocean Eng., vol. 3, World Scientific, Singapore.

- Gallagher, E., S. Elgar, and R. Guza (1998), Observations of sand bar evolution on a natural beach, *J. Geophys. Res.*, *103*, 3203–3215, doi:10.1029/97JC02765.
- Garnier, R., D. Calvete, A. Falqués, and M. Caballera (2006), Generation and nonlinear evolution of shore-oblique/transverse sand bars, *J. Fluid Mech.*, *567*, 327–360.
- Garnier, R., D. Calvete, A. Falqués, and N. Dodd (2008), Modelling the formation and the long-term behavior of rip channel systems from the deformation of a longshore bar, *J. Geophys. Res.*, *113*, C07053, doi:10.1029/2007JC004632.
- Garnier, R., A. Falqués, D. Calvete, J. Thiébot, and F. Ribas (2013), A mechanism for sandbar straightening by oblique wave incidence, *Geophys. Res. Lett.*, *40*, 2726–2730, doi:10.1002/grl.50464.
- Gonzalez-Rodriguez, D., and O. S. Madsen (2011), Boundary-layer hydrodynamics and bedload sediment transport in oscillating water tunnels, *J. Fluid Mech.*, *667*, 48–84.
- Grant, W. D., and O. S. Madsen (1986), The continental-shelf bottom boundary layer, *Annu. Rev. Fluid Mech.*, *18*(1), 265–305.
- Henderson, S., J. Allen, and P. Newberger (2004), Nearshore sandbar migration predicted by an eddy-diffusive boundary layer model, *J. Geophys. Res.*, *109*, C06024, doi:10.1029/2003JC002137.
- Hoefel, F., and S. Elgar (2003), Wave-induced sediment transport and sandbar migration, *Science*, *299*, 1885–1887, doi:10.1126/science.1081448.
- Hsu, T.-J., and B. Raubenheimer (2006), A numerical and field study on inner-surf and swash sediment transport, *Cont. Shelf Res.*, *26*(5), 589–598, doi:10.1016/j.csr.2006.02.004.
- Hsu, T.-J., S. Elgar, and R. Guza (2006), Wave-induced sediment transport and onshore sandbar migration, *Coastal Eng.*, *53*, 817–824, doi:10.1016/j.coastaleng.2006.04.003.
- Jumars, P. A., and A. R. Nowell (1984), Fluid and sediment dynamic effects on marine benthic community structure, *Am. Zool.*, *24*(1), 45–55.
- Kovacs, A., and G. Parker (1994), A new vectorial bedload formulation and its application to the time evolution of straight river channels, *J. Fluid Mech.*, *267*, 153–183.
- Ledwell, J., A. Watson, and S. Law (1998), Mixing of a tracer in the pycnocline, *J. Geophys. Res.*, *103*, 21,499–21,529, doi:10.1029/98JC01738.
- MacMahan, J., E. Thornton, A. Reniers, T. Stanton, and G. Symonds (2008), Low-energy rip currents associated with small bathymetric variations, *Mar. Geol.*, *255*, 156–164.
- Madsen, O. S. (1994), Spectral wave-current bottom boundary layer flows, *Proc. Int'l. Conf. Coastal Eng.*, *1*(24), doi:10.9753/icce.v24.
- Meyer-Peter, E., and R. Müller (1948), Formulas for bed-load transport, in *Proceedings Second Meeting International Association Hydraulic Structures Research*, pp. 39–64, IAHR, Stockholm, Sweden.
- Moulton, M., S. Elgar, and B. Raubenheimer (2014), Improving the time resolution of surfzone bathymetry using in situ altimeters, *Ocean Dyn.*, *64*(5), 755–770, doi:10.1007/s10236-014-0715-8.
- Nielsen, P. (1992), *Coastal Bottom Boundary Layers and Sediment Transport*, Adv. Ser. on Ocean Eng., vol. 4, World Scientific, Singapore.
- Nielsen, P. (2006), Sheet flow sediment transport under waves with acceleration skewness and boundary layer streaming, *Coastal Eng.*, *53*(9), 749–758.
- Plant, N., R. Holman, and M. Freilich (1999), A simple model for interannual sandbar behavior, *J. Geophys. Res.*, *104*, 15,755–15,776, doi:10.1029/1999JC900112.
- Ribberink, J. (1998), Bed-load transport for steady flows and unsteady oscillatory flows, *Coastal Eng.*, *34*(1–2), 59–82.
- Ruessink, B., I. van Enckevort, K. Kingston, and M. Davidson (2000), Analysis of observed two- and three-dimensional nearshore bar behavior, *Mar. Geol.*, *169*, 161–183.
- Shields, A. (1936), Application of similarity principles and turbulence research to bed-load movement (translation of original German by W. P. Ott and J. C. van Uchelen, California Inst. Tech.), *Mitteilungen der Preussischen Versuchsanstalt für Wasserbau und Schiffbau*.
- Soulsby, R. (1997), *Dynamics of Marine Sands: A Manual for Practical Applications*, Thomas Telford, London, U. K.
- Soulsby, R. L., and J. S. Damgaard (2005), Bedload sediment transport in coastal waters, *Coastal Eng.*, *52*(8), 673–689, doi:10.1016/j.coastaleng.2005.04.003.
- Thornton, E., R. Humiston, and W. Birkemeier (1996), Bar/trough generation on a natural beach, *J. Geophys. Res.*, *101*(C5), 12,097–12,110, doi:10.1029/96JC00209.
- Trowbridge, J., and D. Young (1989), Sand transport by unbroken water-waves under sheet flow conditions, *J. Geophys. Res.*, *94*(C8), 10,971–10,991, doi:10.1029/JC094iC08p10971.
- van de Kreeke, J., S. Hoogewoning, and M. Verlaan (2002), An analytical model for the morphodynamics of a trench in the presence of tidal currents, *Cont. Shelf Res.*, *22*(11–13), 1811–1820, doi:10.1016/S0278-4343(02)00039-0.
- van Enckevort, I., and B. Ruessink (2003), Video observations of nearshore bar behaviour. Part 2: Alongshore non-uniform variability, *Cont. Shelf Res.*, *23*, 513–532.